Radionuclide spatial distribution and dose deposition for *in vitro* assessments of ^{212}Pb-αVCAM-1 targeted alpha therapy

Short title: Dosimetry in *in vitro* assessment of TAT

Anne-Marie Frelin-Labalme[1], Thomas Roger[1], Nadia Falzone[2], Boon Quan Lee[2], Nicola R. Sibson[2], Katherine A. Vallis[2], Myriam Bernaudin[3], Samuel Valable[3] and Aurélien Corroyer-Dulmont[2,3].

[1] Grand accélérateur National d'Ions Lourds (GANIL), CEA/DRF-CNRS/IN2P3, Boulevard Henri Becquerel, 14076 Caen, France

[2] CR-UK/MRC Oxford Institute for Radiation Oncology, Department of Oncology, University of Oxford, Oxford, United Kingdom

[3] Normandie Univ, UNICAEN, CEA, CNRS, ISTCT/CERVOxy group, Caen, France

E-mail: anne-marie.frelin@ganil.fr

Radionuclide spatial distribution and dose deposition for *in vitro* assessments of ^{212}Pb-αVCAM-1 targeted alpha therapy

Abstract.

Purpose. Targeted alpha therapy (TAT) takes advantage of the short-range and high linear-energy-transfer of α-particles and is increasingly used, especially for the treatment of metastatic lesions. Nevertheless, dosimetry of α-emitters is challenging for the very same reasons, even for *in vitro* experiments. Assumptions, such as the uniformity of the distribution of radionuclides in the culture medium, are commonly made, which could have a profound impact on dose calculations. In this study we measured the spatial distribution of α-emitting ^{212}Pb coupled to an anti-VCAM-1 antibody (^{212}Pb-αVCAM-1) and its evolution over time in the context of *in vitro* irradiations.

Methods. Two experimental setups were implemented without cells to measure α-particle count rates and energy spectra in culture medium containing 15 kBq of ^{212}Pb-α-VCAM-1. Silicon detectors were placed above and below cell culture dishes for 20 hours. One of the dishes had a 2.5-µm-thick mylar-base allowing easy detection of the α-particles. Monte Carlo simulations were performed to analyze experimental spectra. Experimental setups were modelled and α-energy spectra were simulated in the silicon detectors for different decay positions in the culture medium. Simulated spectra were then used to deconvolute experimental spectra to determine the spatial distribution of ^{212}Pb-αVCAM-1 in the medium. This distribution was finally used to calculate the dose deposition in cell culture experiments.

Results. Experimental count rates and energy spectra showed differences in measurements taken at the top and the bottom of dishes and temporal variations that did not follow ^{212}Pb decay. The radionuclide spatial distribution was shown to be composed of a uniform distribution and concentration gradients at the top and the bottom, which were subjected to temporal variations that may be explained by gravity and electrostatic attraction. The absorbed dose in cells calculated from this distribution was compared with the dose expected for a uniform and static distribution and found to be 1.75 times higher, which is highly significant to interpret biological observations.

Conclusion. This study demonstrated that accurate dosimetry of α-emitters requires the experimental determination of radionuclide spatial and temporal distribution and highlighted that *in vitro* assessment of dose for TAT cannot only rely on a uniform distribution of activity in the culture medium. The reliability and reproducibility of future experiments should benefit from specifically developed dosimetry tools and methods.

Key Words: ^{212}Pb, in vitro irradiations, α-emitters, targeted alpha therapy, dosimetry, clonogenic assay

1. Introduction

Current practices for the treatment of primary resectable cancer is very effective. However in many cases, cancer cells spread beyond the primary tumour making treatment therapeutically challenging, often resulting in poor outcomes. In this context, targeted α-therapy (TAT) has showed great potential in treating systematically diffuse cancer and metastatic lesions. Alpha particles have the advantage of a short range, well adapted to sub-millimeter tumors (100 µm or less), a high linear energy transfer (LET) and a potent cytotoxicity. Importantly, TAT is not affected by tissue oxygen levels[1,2] or dose rate effect. This is of particular interest in cancer treatment, as it is known that a significant proportion of cancers present a hypoxic microenvironment which affects the efficacy of radiotherapy[3,4]. These favorable properties explain the increasing development and use of TAT[5], and the recent introduction of a novel radiopharmaceutical, bone-seeking α-emitter ^{223}Ra (Xofigo®), for the treatment of metastatic prostate cancer[6,7].

The development of new radiopharmaceuticals goes along with preclinical studies assessing their efficiency in tumor control as well as toxic effects in healthy tissues. It is also highly desirable to compare their effects to other radiotherapy treatments such as x-Ray external beam radiotherapy (EBRT) or β-emitting targeted radiotherapy[8]. It is thus necessary to have an accurate knowledge of the activity administered to the biological sample and of the mean absorbed dose to the cells per unit time-integrated activity (S-values)[9-12]. *In vitro* dosimetry in TAT is particularly challenging because of the short range of α-particles and the µm diameter of cell cultures. In this configuration, the fraction of energy emitted by the radioactivity that is absorbed by the cells depends on many parameters and is poorly known.

Consequently, studies evaluating the biological effects through *in vitro* experiments are based on a number of assumptions, such as a uniform distribution of the radionuclides in solution. While these assumptions might be reasonable for radionuclides emitting β-particles in the mm to cm range, they can strongly affect the accuracy of dosimetry in *in vitro* irradiations performed with α-emitters.

This work formed part of a preclinical study that evaluated the therapeutic potential of TAT, combining an α-emitting radionuclide (^{212}Pb) to an anti-VCAM-1 antibody (^{212}Pb-αVCAM-1). The upregulation of vascular adhesion molecule (VCAM-1) has been shown to be specific to early stage brain metastases[8,13-15]. The objective of the present study was thus to perform accurate and reliable dosimetry for *in vitro* irradiations with ^{212}Pb-αVCAM-1. The first step of this work was the experimental determination of the spatial distribution of radionuclides in culture medium using α energy spectra measurements and Monte Carlo (MC) simulations. These data allowed the determination of the fraction of α-particles emitted by the radioactivity absorbed by the cells. In a second step, MC simulations were performed to determine the average dose deposited in cells per emitted α-particle, allowing the calculation of S-values and the absorbed dose to the cells for the experimental conditions.

2. Materials and methods

An experimental setup and MC simulations were implemented to measure the spatial distribution of the α-emitting ^{212}Pb-αVCAM-1 in the context of *in vitro* irradiations and to calculate the corresponding dose deposition in cells.

2.1. Conjugation and radiolabeling of targeted alpha-particle therapeutic ^{212}Pb-αVCAM-1

^{212}Pb (Orano-Med, Bessines-sur-Gartempes, France) was conjugated to VCAM-1 using a protocol based on previous publications[16,17]. The metal chelator, TCMC (Macrocyclics, Plano, USA) was conjugated in 15-fold molar excess with the VCAM-1 antibody, resulting in a ligand to antibody ratio of 2. One mg of TCMC-VCAM-1 was then incubated for 30 min with 37 MBq of ^{212}Pb at 37°C. Using instant thin layer chromatography (iTLC) the radiolabelling yield was found to be 93.5%. The solution was re-suspended in PBS before being added to the wells of a six-well plate.

2.2. In vitro assessment of the ^{212}Pb-αVCAM-1 radiopharmaceutical

^{212}Pb, which has a 10.6 hours half-life, does not itself emit α-particles but produces ^{212}Bi (60.5 minutes half-life) through β-decay. Two decay paths can then be followed by ^{212}Bi that will lead to the emission of α-particles of 6.1 and 8.8 MeV with respective probabilities of 36 and 64 %. These particles have respective projected ranges of 50 and 91 µm in water and LET reaching 226 keV/µm along their path[18]. The whole decay chain of ^{212}Pb also generates the emission of β-particles, photons (γ- and x-rays) and Auger electrons. The electrons emitted during the decay chain (β-particles, Auger, or secondary electrons produced by photons) present LET values below 2.3 keV/µm in all cases.

VCAM-1 has previously been shown to be upregulated on the surface of endothelial cells[14,15] and in a recent study, it has been used to target brain micrometastases. ^{212}Pb-αVCAM-1 was evaluated in clonogenic assays with MDA cells which don't express VCAM-1. Consequently the dose deposited in cells was only the result of the cells thickness and the radioisotopes distribution and decay, as there was no specific-binding between the cells and the antibody.

2.3. Experimental α-particle count rates and energy spectra

The α-particle spectra were measured by silicon detectors placed in two different configurations, represented in figure 1. Culture medium containing 15 kBq of ^{212}Pb-α-VCAM-1 was added about 8 hours after the conjugation to each test well, at an initial time *t = 0 min*. The injected activity was obtained by diluting the initial solution which activity was measured from the 238.6 keV γ-peak (energy window 50-300 keV) of the ^{212}Pb decay with a Gamma counter Cobra (GMI-INC, USA). Measurements were performed without cells with a depth of 1.8 mm of medium in each well. This configuration is quite representative of our clonogenic assay where the cells don't express VCAM-1. In the first setup (CH1 corresponding to the acquisition channel 1), a custom-made well was placed 1 mm above a silicon detector. The dish base consisted of a 2.5 µm polyester film (mylar), much thinner than the range of α-particles, thus allowing their transmission toward the detector. This setup allowed the detection of the activity located at the bottom of the culture medium. In the second configuration (CH2), the silicon

detector was placed above a TTP tissue culture test plate (Dutscher), commonly used in biological experiments, with a diameter of 21.6 mm and height of 20 mm. This configuration provided a second independent measurement of the α-spectra. In this setup the detector was sensitive to radioactivity located in the upper part of the medium (i.e. from the surface to a few tens of µm in depth).

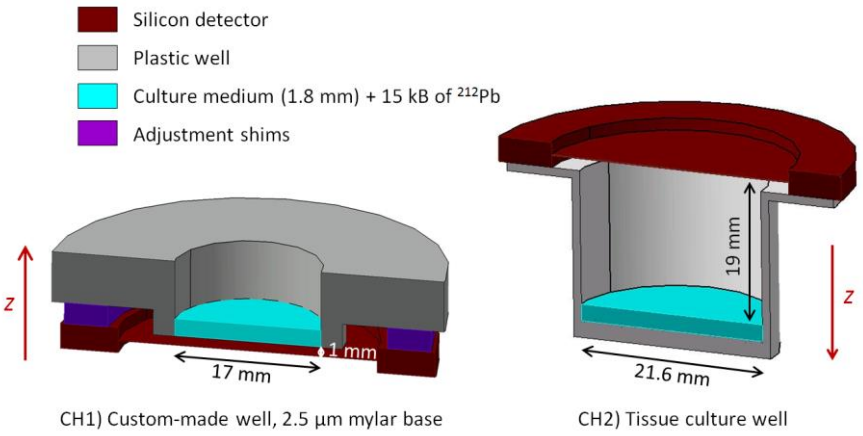

Figure 1. Cross section of the experimental setups. In the first configuration (CH1), a custom made well with a mylar base of 2.5 µm thickness, was placed 1 mm above a silicon detector. In the second configuration (CH2), the detector was placed above a standard culture well (from 6-well plate) of 21.6 mm diameter and 20 mm height. The distance between the culture medium surface and the active area of the silicon detector was 19 mm.

Both setups were implemented in a light-tight box at room temperature about 20 °C). The silicon detectors used (MSD026-150 commercialized by Micron Semiconductor Ltd, UK), were 144 µm thick, which is greater than the range of α-particles in silicon but small relative to the range of electrons, thus making them insensitive to emissions other than α-particles. Given the α particles energy and the relatively low counting rate, the detection efficiency was 100 %. The detectors were connected to preamplifiers and a FASTER acquisition system which recorded the energy and the arrival time of each particle that reached the detectors during a 20 hour period. The measurement chain was calibrated in energy with the two α emission peaks at 6.1 and 8.8 MeV.

Signal measurements were processed after this time period to determine the experimental count rates and energy spectra for both configurations over time. Integration times of 100 s were used in the first 15 minutes (to achieve a high initial time resolution) and 600 s thereafter.

Alpha particles emitted by the radionuclides inside a material are continuously attenuated until they exit. Consequently, the energy spectrum measured from a material containing ^{212}Pb isotopes will not present the original 2 peaks at 6.1 and 8.8 MeV, but a continuum of lower energies. The analysis of this spectrum allows the determination of the material thickness crossed by the different α-particles, and thus their emission position.

2.4. Simulated energy spectra

Monte Carlo simulations were performed using GATE (Geant4 Application for Tomographic Emission)[19] v8 to study the evolution of α-particle spectra measured by the silicon detectors according to the position of α-emission. For that purpose, the geometry and materials of the experimental setups (represented in figure 1) were modelled. Culture medium was represented as water.

As the detectors are insensitive to β-particles and photons, the ^{212}Pb decay chain was simulated by the corresponding α-energy spectrum only (1 simulated α-particle corresponding to 1 decay). The ^{212}Pb spatial distribution was assumed to be solely a function of the distance *z* between the particle emission position and the medium surface (distance from the bottom of the dish in the case of CH1 and from the surface of the medium in the case of CH2 as shown by the z axes in figure 1). Cylinder sources of the same diameter as the culture medium and 2 µm thick were simulated at different distances z_i, ranging from 0 to 90 µm in 2 µm increments, in the culture medium. The number of α particles recorded in the silicon volume decreases with the distance because of the geometrical efficiency and the increasing thickness of water between the source and the silicon volume. Consequently, the number of primary particles was increased from 1×10^5 to 6.6×10^6 between 0 and 90 µm respectively.

The energy spectra $SP_{MC}(z_i, E)$ were recorded in the silicon detector volume for every source distance z_i.

2.5. Spatial distribution of radionuclides

The spatial distribution of ^{212}Pb-αVCAM-1 was determined at the top and the bottom of the culture medium at different times *t (min)* as informed by the experimental and simulated spectra acquired as described above. Experimental spectra of the energy deposited in the silicon detectors were generated by α-particles emitted from different positions in the culture medium. Subsequent MC simulations were performed to determine the energy spectra $SP_{MC}(z_i, E)$, corresponding to particular positions z_i *(μm)*, *E(MeV)* arising from the energy deposited in the detector. It is then possible to combine these individual spectra to describe the spectrum generated by a complex isotope spatial distribution:

$$SP(t,E) = \sum_i A(t,z_i) \cdot SP_{MC}(z_i,E) \quad (1)$$

with $A(t, z_i)$ the α-emitter spatial distribution at time *t*.

This distribution was assumed to be composed of a uniform distribution *h(t)* and an exponential concentration gradient defined by *a(t)* and *b(t)*:

$$A(t,z_i) = h(t) + a(t) \cdot e^{-b(t)\cdot z_i} \quad (2)$$

The variability of the *b* parameter allows describing very different distributions from an almost linear gradient ($b<<1$) to a sharp gradient at the surface ($b>>1$). These three parameters, and thus the radionuclide spatial distribution, were determined at each measurement time by minimizing the χ^2 parameter between *SP(t, E)* and the experimental spectrum $SP_{expe}(t, E)$ measured in section 2.1.

2.6. Absorbed radiation dose to cells

The calculation of the absorbed radiation dose to the cells is based on the fraction of energy imparted by the α-particles in cells. This factor depends not only on the LET of particles reaching the cells, but also on the cell thickness. Consequently, absorbed dose calculations were divided into two steps: the

measurement of the cell thickness by two-photon imaging and the MC simulation of dose deposition by α-particles in cells.

Cell thickness measurement

In vitro tumor cell thickness was evaluated using two-photon imaging. Cells were plated in 6-well plates (750 cells/well). The next day, two-photon imaging was performed on a Leica DM6000 stand (CYCERON biomedical imaging platform) with a 25x/0.95 water HCXIRAPO objective and laser excitation wavelength centered at 900 nm. A total of 8 cells were evaluated and cell thickness determined using ImageJ software[20] and PMOD 3.1 software.

Simulation of the fraction of deposited energy

The CH1 simulation setup was modified by removing the silicon detector and replacing the mylar base with a 2 mm thick plastic base. A cylindrical volume of water representing a monolayer cell culture, whose thickness was measured in the previous section, was simulated below the culture medium. As in section 2.3, a cylindrical α-source of the same diameter as the culture medium and 2 µm thick was simulated in the culture medium at different distances from the cells. For each distance z_i, the mean dose deposited in the cell volume per α-particle, $S(z_i)$, was thus determined. Finally the absorbed dose rate to cells $\frac{dD}{dt}(t)$ deposited by the whole radionuclide distribution was calculated:

$$\frac{dD}{dt}(t) = \sum_i A(t, z_i) \cdot S(z_i) \qquad (3)$$

with $A(t, z_i)$ the spatial distribution of radionuclides determined in the previous section. This dose deposition was compared to uniform and static distributions of the same activity (15 kBq at *t =0 min*).

3. Results and discussion

3.1. Experimental α-particle count rates and energy spectra

Experimental count rates are represented in figure 2 (A) and (B) with the count rates expected assuming (as is normally done) a static and uniform radionuclide distribution. These results highlight that experimental count rates are higher than those based on common assumption in both configurations. In the case of CH1, there is a substantial difference in count rate with a significant increase in the count rate during the first 180 minutes of addition of radioactivity to the medium. After that time, the behavior progresses toward the predicted ^{212}Pb decay rate, although the decrease constant remains smaller than the ^{212}Pb decay constant ($8.97 \cdot 10^{-4}$ min^{-1} versus $1.09 \cdot 10^{-3}$ min^{-1}). In the case of CH2, contrary to CH1, a fast decay is observed during the first few minutes. After that, the decrease becomes exponential with a constant comparable to the ^{212}Pb decay constant ($1.06 \cdot 10^{-3}$ min^{-1}).

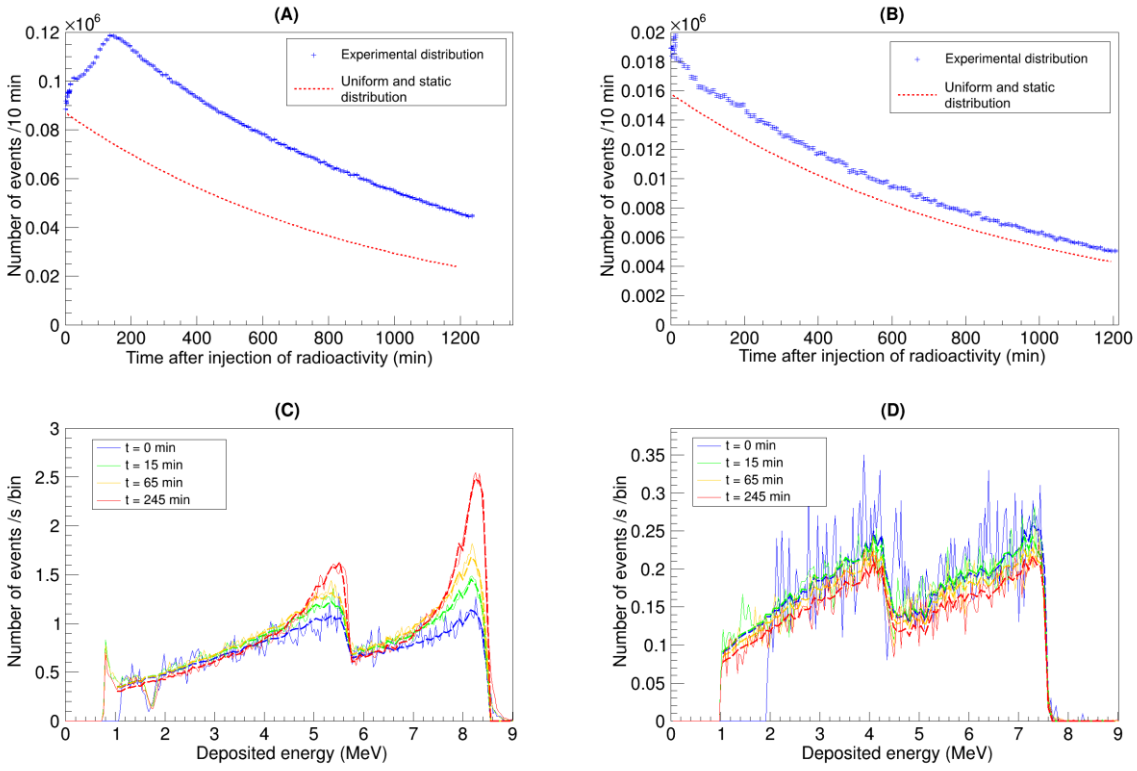

Figure **2.** (A) and (B): count rates measured as a function of post-injection time in both configurations and compared to the count rates expected for a static and uniform distribution. (A) corresponds to the CH1 setup and (B) to the CH2 setup. (C) and (D): energy spectra measured at 0, 15, 65 and 245 min respectively in CH1 and CH2 setups (plain lines) and convoluted spectra (bold dashed lines).

Experimental spectra are represented in light colors in figure 2 (C) and (D). For clarity, only the spectra measured at 0, 15, 65 and 245 min are displayed but similar results were obtained at all measurement times. Energy spectra show differences between both configurations. Indeed, because of the lower count rate in CH2 (due to the larger distance between the culture medium and the detector), spectra measured in this configuration have a lower signal to noise ratio. It can also be seen that because of the 19 mm of air crossed by particles in CH2 (compared to 1 mm in CH1), the maximum energy recorded in CH2 is lower than in CH1 (respectively 7.7 and 8.6 MeV). More importantly, the two configurations result in spectra of significantly different shapes, indicative of differences in isotope distributions at the top and the bottom of the culture medium. Finally, the shape of the spectra measured in CH1 clearly shows variations over time, which indicate temporal modifications of the spatial distribution and are in agreement with the count rate measurements.

3.2. Energy spectra Monte Carlo simulations

The MC energy spectra of α particles emitted at 0, 10, 20, 40 and 60 µm from the surface, necessary to determine the ^{212}Pb-αVCAM-1 spatial distribution, are represented figure 3. For clarity, other spectra are not represented. The largest relative statistical uncertainties on the number of particles recorded in the silicon volume were 0.6 % for CH1 and 1.5 % for CH2. They clearly show the moderation of α particles by increasing thicknesses of medium. They also show the effect of the more important thickness of air in the CH2 setup, leading to a lower maximal energy deposited in the silicon detector.

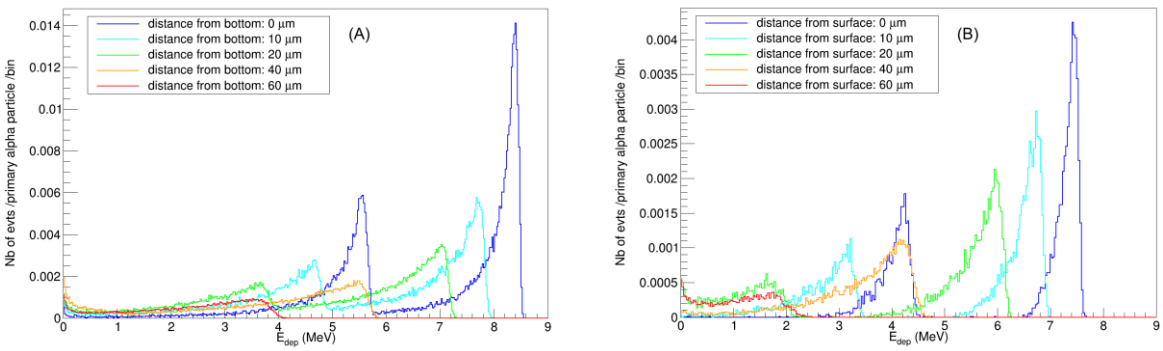

Figure 3. Energy spectra simulated in both configurations (CH1 and CH2) for alpha particles emitted from different depths.

3.3. Radionuclide spatial distribution

The convoluted spectra, given by Eq. (1) were determined by χ^2 minimization with experimental spectral. They are represented in dashed lines in the lower part of figure 2, and show very good agreement with experimental spectra for all measurement times. The corresponding spatial distributions, determined by this method at 0, 15, 65 and 245 min, are represented in figure 4. The direction of *z* was inverted for CH2 in order to represent in the same figure both extremities of the distribution of the ^{212}Pb-αVCAM-1 in the culture medium. It is not possible to record the distribution in the middle of the dish because of the short α-particle range. Figure 4 shows that the uniform distributions measured in these two independent configurations are very close (about 16 particles emitted per second by each 2 µm thick slice of culture medium for CH1, and 18 particles emitted per second for each 2 µm thick region for CH2). However, the concentration gradients are quite different when comparing the lower and upper parts of the distribution. The gradient at the base of the dish (CH1) extends to about 10 µm and its intensity increases with time relative to the uniform distribution. The gradient at the top (CH2) is narrower (about 4 µm) and the intensity is almost constant over time.

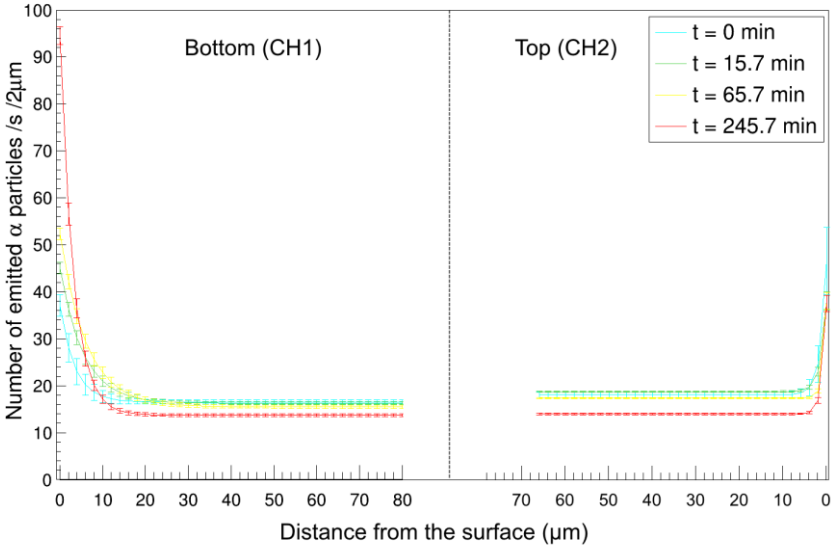

Figure 4. ^{212}Pb-VCAM1spatial at the bottom and the top of the culture medium at different measurement times.

The evolution of the spatial distribution was analyzed more closely through the parameters *h(t)*, *a(t)* and *b(t)*, represented in figure 5.

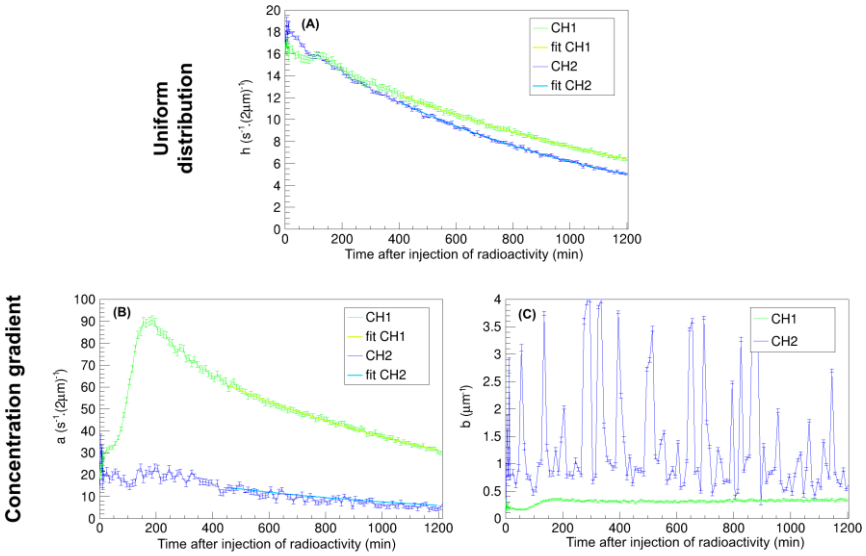

Figure 5. Evolution of $\boldsymbol{h(t)}$, $\boldsymbol{a(t)}$ and $\boldsymbol{b(t)}$ for both configurations

As already shown in figure 4, the uniform distributions, represented in the upper part of figure 5 have comparable values for the two experimental configurations, CH1 and CH2, which is consistent with the identical activity injected in both configurations. In CH1, an initial phase shows a decrease followed by a slight increase in α-particle emission rate up to t = 120 min. After 120 min, both uniform distributions return to an exponential behavior, with a decrease constant of $8.8 \cdot 10^{-4}$ min^{-1} for CH1, smaller than the ^{212}Pb decay constant, and $1.05 \cdot 10^{-3}$ min^{-1} (comparable to the ^{212}Pb decay constant) for CH2. This points to the migration of radionuclides toward the lower part of the dish over time, compensating for radionuclide decay.

The concentration gradient, described by *a(t)* (indicating the gradient intensity) and *b(t)* (indicating its spatial extension) is represented in the lower part of figure 5. In the case of CH1, the significant increase of *a(t)* during the first 180 minutes shows that the count rate augmentation observed in figure 2 is due to a marked increase in the concentration gradient in the lower part of the dish during the first 180

minutes. This increase shows two phases before 50 and 180 minutes. The evolution of *b(t)* shows an increase after about 75 min, before a stabilization around 150 min, which indicates a reduction of the gradient extension at the beginning of the irradiation. After t = 180 min, the intensity follows an exponential decrease with a constant of 8.92 10^{-4} min^{-1}. As for the uniform distribution, this is smaller than the ^{212}Pb decay constant, indicating that the radionuclide distribution is not static but continues to contribute to the formation of a gradient after 180 min, even if at a slower rate, compensating for the decay of ^{212}Pb.

In the case of CH2, the magnitude of the gradient intensity is about 4-fold smaller than for CH1. Despite the greater amount of noise, it can be seen that the gradient intensity decreases during the first 120 min, before following exponential behavior with a decrease constant of $1.14 \cdot 10^{-3}$ min^{-1} which is of the same order as the decay constant of ^{212}Pb. The evolution of *b(t)* in CH2 is subjected to very significant variations owing to the high noise measured in this configuration and, subsequently, a less accurate χ^2 minimization. Nevertheless, these values reveal sharper gradients than in CH1 irrespective of the time.

For dosimetry considerations, the spatial distribution $A(z_i, t)$ measured over time for CH1 provides the fraction of the 15 kBq of radioactivity to which cells would be exposed in these irradiation conditions.

3.4. Dose deposition in cells

Cell thickness measurement

The determination of cell thickness was performed on two-photon images of tumor cells; examples shown in figure 6. The measurements performed on the side view provided a mean thickness of 20.25 µm with a standard deviation of 1.82 µm.

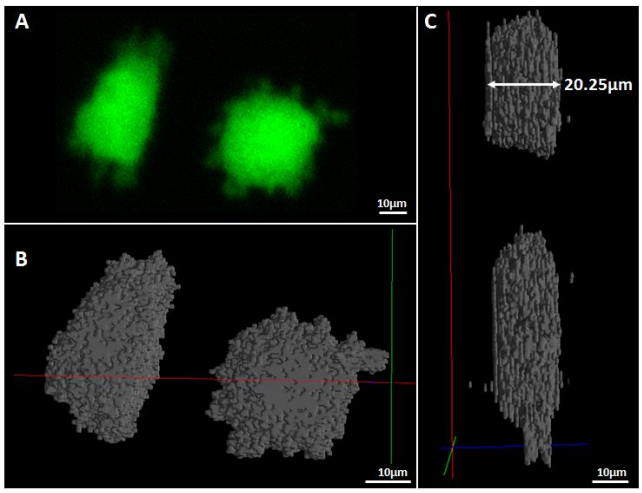

Figure 6. Tumor cell thickness two-photon imaging evaluation. (A) Representative two-photon imaging of two GFP positive tumor cells. (B) 3D view from the bottom of the two representative tumor cells. (C) 3D view from the left of the two representative tumor cells.

Fraction of deposited energy simulation

The MC simulations performed with the experimental cell thickness allowed the determination of the dose deposited in cells (modelled as a 20 µm thick cylindrical volume of water) per emitted α-particle, represented in figure 7 A) as a function of the emission position ($S(z_i)$). The absorbed dose rate generated by the spatial distribution of radioactivity measured in section 3.3 is then represented in figure 7 B) as a function of time following addition of radioactivity to cells and compared to the dose rate expected for a uniform and static distribution. These two curves, similar to the count rates displayed in figure 2 for CH1, show important discrepancies.

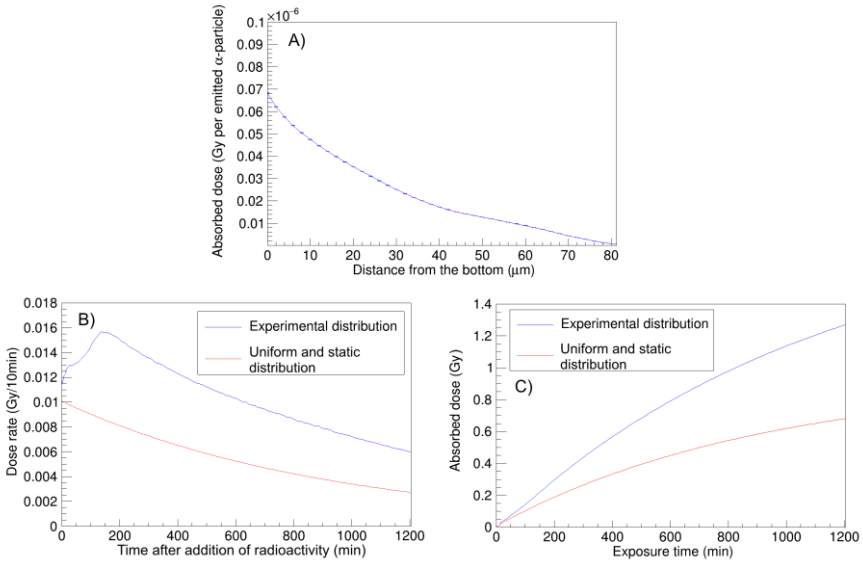

Figure 7. Dose deposited by alpha particles in a 20 µm thick cylindrical volume of water representing cell culture. A) Dose deposited per emitted α-particle according to the emission position. B) Dose deposited in 10 minutes by the experimental spatial distribution and a uniform and static distribution as a function of time. C) Absorbed dose as a function of exposure time for the experimental and a uniform and static distribution.

The corresponding cumulative doses are represented in figure 7 C) as a function of exposure time and show differences between cumulative doses increasing with exposure time. The doses corresponding to a 4 hour irradiation are 0.35 Gy for the experimental spatial distribution and 0.20 Gy for the uniform and static distribution, which corresponds to a 42 % error.

4. Discussion

This study presents the spatial distribution measurements of an α-emitter in the context of a typical *in vitro* irradiation. The study was performed with two independent setups (a custom-made well with α-particle detection from below, and a commercially available well with particle detection from above) allowing detection of the changing distribution of ^{212}Pb-αVCAM-1 in the culture medium over 20 hours. Both configurations provided comparable results, thus indicating good experimental reliability. Nevertheless, the count rates measured in both setups were higher than those expected for a uniform and static distribution. This may indicate a lower activity at the middle of the culture medium but could also

be explained by an inaccurate measurement of the activity initially injected. This should be investigated in further experiments.

Data analysis, by means of MC simulation, showed that the spatial distribution of radionuclides was composed of a homogenous part and a concentration gradient oriented toward the surfaces of the medium (the bottom in the case of CH1 and the top in the case of CH2). The homogenous component was found to be of the same order of magnitude in both configurations. After a first decrease phase observed in CH1 before t = 120 min, a migration of radionuclides toward the bottom was observed. This migration was significant and may be explained by the migration of ^{212}Pb-αVCAM-1 molecules, due to gravity or electrostatic attraction to the mylar surface. Concentration gradients were also analyzed at both extremities of the culture medium. At the top, the gradient spatial extension was limited to about 4 µm and its intensity followed ^{212}Pb decay. This concentration gradient can be explained by a meniscus at the surface of the liquid. The concentration gradient observed in the lower part of the dish was much more marked, in terms of spatial extension (about 10 µm) and intensity. Moreover, *a(t)* showed three different phases: two increasing phases before t =50 min and t = 180 min, and an exponential decrease after 180 minute, slower than the ^{212}Pb decay. It is possible that the first fast phase may be explained by electrostatic attraction, whereas the slower phase after t = 180 min may be explained by gravity combined with the physical limit of the mylar base. Further investigations with molecules presenting different characteristics (free ^{212}Pb for instance) could provide more insight on the displacements in the culture medium.

This experiment, performed without cells, proves the extreme complexity of radiopharmaceutical kinetics during *in vitro* assessment and the huge consequence on dosimetry. The complex kinetics described above are very dependent on the experimental conditions and various parameters could change the results of this study. Indeed, it can be assumed that the electrostatic attraction of the mylar was different from a standard culture dish, or that the temperature and humidity inside an incubator may change the culture medium viscosity or its evaporation. Similarly, a single activity level (15 kBq) was tested in this work, while the activity concentration could have an impact on the kinetics.

Hence, even though the assessment of the temporal and spatial distribution of radionuclides described here is much more representative of our *in vitro* experiments than the commonly applied assumption of uniformity of distribution (because cancer cells don't express VCAM-1), it primarily shows the magnitude of error in dose calculation during in vitro experiments. The comparison of the absorbed dose with the one expected for a uniform and static distribution, highlights the significant discrepancies in current methodologies assuming uniform and static activity distributions. In turn, this leads to a major concern for the quantitative interpretation of radiobiology experiments. Indeed, the inaccuracy of absorbed dose calculation could inevitably bias the preclinical assessment of TAT and makes comparison with β-emitters treatments (whose longer range and lower LET imply different *S*-values) impossible.

In the case of specific-biding of the radiopharmaceutical to receptors on the cells surfaces or internalization into the cells, the kinetics is even more complex. Indeed, it is determined by the interactions between the cells and the antibody, but also the stability of the chemical bound between the chelator and the radioisotope (in particular in the case of α-emitters). The impact of gravity and electrostatic mechanisms on dose deposition is then certainly much less significant. Experimental dosimetry is thus even more necessary for clonogenic assays of specific-binding radiopharmaceuticals, and must absolutely be performed with cells. To answer that issue, the experimental setup presented in this study could be implemented in *in vitro* experiments with customized culture wells. Indeed, experimental energy spectra of α-particles combined with appropriate MC simulations, would provide the spatial and temporal distribution of α-emitting radioisotopes, thus taking into account internalization or unbound isotopes for instance. Further studies are thus necessary to improve the dosimetry of short range particle emitters (α particles or Auger electrons).

To advance towards microdosimetry and improved biophysical models[21,22], the spatial distribution of the radiopharmaceutical in the culture medium should be completed by evaluation of the subcellular distribution. The imaging techniques described here to determine the cells thickness, could be expanded to fluorescence tagged antibodies of VCAM-1 to provide the activity distribution as a function of depth

in the cell layer. These measurements could then be combined with a more realistic geometry of cells to determine specific energy loss in the different cell compartments.

5. Conclusion

This study presents the experimental determination of the spatial distribution of ^{212}Pb-αVCAM-1 in solution and provides a calculation of *S*-values and absorbed dose for α-particles in classical *in vitro* irradiations, typical of those used for clonogenic assays. The results demonstrate the problems associated with the assumption of a uniform and static spatial distribution of activity during cell exposure, and the unsuitability of methods used with β-emitters. Indeed, assuming uniform and static spatial distributions leads to significant errors in absorbed dose calculation and, consequently, in the quantification of biological effects. This issue prevents the comparison of treatment efficacy with other experiments or treatments. The measurements of this study, performed without cells, are quite representative of our ^{212}Pb-αVCAM-1 clonogenic assays. Nevertheless *in vitro* experiments implying specific-binding with the cells should necessarily require measurements in presence of cells. Future experiments performed with short-range particle emitters should thus rely on spatial distribution measurements of the activity and an accurate assessment of cell thickness to ensure accurate interpretation.

Acknowledgements

The authors would like to thank the LPC Caen for the loan of FASTER acquisition module and Dr. Elisa Grimoin for the help with the two-photon imaging system. CNRS, CEA, Université de Caen-Normandie, the French Ministère de l'Enseignement Supérieur et de la Recherche, the Conseil Régional-Normandie and the European Union-Fonds Européen de Développement Régional (FEDER), the Fédération pour la Recherche sur le Cerveau par l'opération Rotary "Espoir en tête » (FRC), ANR-11-LABEX-0018-01 ; ANR-10-EQPX1401. MSS, NRS, KAV, OT and NF were supported by Cancer Research UK (grant number C5255/A15935). Grant support was also received from the Medical Research Council (MC_PC_12004) (KAV, OT, NF), the Engineering and Physical Sciences Research Council (EPSRC)

Oxford Centre for Drug Delivery Devices (EP/L024012/1) (KAV), the CRUK Oxford Centre (OT) and the CRUK/EPSRC Cancer Imaging Centre Oxford (C5255/A16466) (KAV).

References

1. G. Sgouros, Alpha-particles for targeted therapy. *Adv Drug Deliv Rev.* 2008; 60(12):1402-1406. doi: 10.1016/j.addr.2008.04.007

2. M. R. Zalutsky and D. D. Bigner, Radioimmunotherapy with alpha-particle emitting radioimmunoconjugates. *Acta Oncol.* 1996; 35(3): 373-9. PMID: 8679269

3. L. H. Gray, A. D. Conger, M. Ebert, S. Hornsey and O. C. Scott, The concentration of oxygen dissolved in tissues at the time of irradiation as a factor in radiotherapy. *Br J Radiol.* 1953; 312: 638-48. doi: 10.1259/0007-1285-26-312-638

4. M. R. Horsman and J. Overgaard, The impact of hypoxia and its modification of the outcome of radiotherapy. *J Radiat Res*. 2016; 57(S1): i90-i98. doi: 10.1093/jrr/rrw007

5. F. Guerard, J. Barbet, J.-F. Chatal, F. Kraeber-Bodere, M. Cherel and F. Haddad, Which radionuclide, carrier molecule and clinical indication for alpha-immunotherapy. *Q J Nucl Med Mol Imaging*. 2015; 59: 161-167. PMID: 25752501

6. L. Maffioli, L. Florimonte, D. C. Costa et al, New radiopharmaceutical agents for the treatment of castration-resistant prostate cancer. *Q J Nucl Med Mol Imaging*. 2015; 59: 420-438. PMID: 26222274

7. J. Barbet, M. Bardiès, M. Bourgeois et al, Radiolabeled Antibodies for Cancer Imaging and Therapy. *Methods in Molecular Biology*. 2012; 907:681-97. doi: 10.1007/978-1-61779-974-7_38

8. N. Falzone, N. L. Ackerman, L. de la Fuente Rosales et al, Dosimetric evaluation of radionuclides for VCAM-1-targeted radionuclide therapy of early brain metastases. *Theranostics 2018*. 2018; 8(1): 292-303. doi: 10.7150/thno.22217

9. W. E. Bolch, K. F. Eckerman, G. Sgouros and S. R. Thomas, MIRD pamphlet No. 21: a generalized schema for radiopharmaceutical dosimetry--standardization of nomenclature. *J Nucl Med*. 2009; 50(3): 477-84. doi: 10.2967/jnumed.108.056036

10. M. Šefl, K. Pachnerová Brabcová and V. Štěpán, Dosimetry as a Catch in Radiobiology Experiments. *Radiat Res*. 2018; 190(4): 404-411. doi: 10.1667/RR15020.1

11. C.-Y. Huang, S. Guatelli, B. M. Oborn and B. J. Allen, Microdosimetry for targeted alpha therapy of cancer. *Comput Math Methods Med.* 2012; 2012:153212. doi: 10.1155/2012/153212

12. G. Sgouros, J. C. Roeske, M. R. McDevitt et al, MIRD Pamphlet No. 22 (Abridged): Radiobiology and Dosimetry of α-Particle Emitters for Targeted Radionuclide Therapy. *J Nucl Med*. 2010; 51(2): 311-28. 10.2967/jnumed.108.058651

13. V. W. Cheng, M. S. Soto, A. A. Khrapitchev et al, VCAM-1 targeted magnetic resonance imaging enables detection of brain micrometastases from different primary tumours. *Clin Cancer Res*. 2018. doi: 10.1158/1078-0432.CCR-18-1889

14 M. S. Soto, S. Serres, D. C. Anthony and N. R. Sibson, Functional role of endothelial adhesion molecules in the early stages of brain metastasis. *Neuro Oncol*. 2014; 16(4): 540-51. doi: 10.1093/neuonc/not222

15. S. Serres, M. S. Soto, A. Hamilton et al, Molecular MRI enables early and sensitive detection of brain metastases. *Proc Natl Acad Sci U S A*. 2012; 109(17): 6674-9. doi: 10.1073/pnas.1117412109

16. V. Boudousq, L. Bobyk, M. Busson et al, Comparison between Internalizing Anti-HER2 mAbs and Non-Internalizing Anti-CEA mAbs in Alpha-Radioimmunotherapy of Small Volume Peritoneal Carcinomatosis Using 212Pb. *PLOS ONE*. 2013; 8: 1-12. doi: 10.1371/journal.pone.0069613

17. Z. Tan, P. Chen, N. Schneider et al, Significant systemic therapeutic effects of high-LET immunoradiation by 212Pb-trastuzumab against prostatic tumors of androgen-independent human prostate cancer in mice. *Int J Oncol*. 2012; 40(6): 1881-8. doi: 10.3892/ijo.2012.1357

18. N. L. Ackerman, L. de la Fuente Rosales, N. Falzone, K. A. Vallis and M. A. Bernal, Targeted alpha therapy with 212Pb or 225Ac: Change in RBE from daughter migration. *Phys Med.* 2018 ; 51 : 91-98. doi: 10.1016/j.ejmp.2018.05.020

19. D. Sarrut, M. Bardiès, N. Boussion et al, A review of the use and potential of the GATE Monte Carlo code for radiation therapy and dosimetry applications. *Med Phys.* 2014; 41(6): 064301. doi: 10.1118/1.4871617

20. C. A. Schneider, W. S. Rasband and K. W. Eliceiri, NIH Image to ImageJ: 25 years of image analysis. *Nat Methods*. 2012; 9(7): 671-5. PMID: 22930834

21. S. Rahmanian, M. Niklas, A. Abdollahi, O. Jäkel and S. Greilich, Application of fluorescent nuclear track detectors for cellular dosimetry. *Phys Med Biol*. 2017; 62: 2719-2740. doi: 10.1088/1361-6560/aa56b4

22. A. Sadremomtaz and M. Masoumi, Cellular dosimetry of different radionuclides for targeted radionuclide therapy: Monte Carlo simulation. *Biomed Phys Eng Express*. 2018; 4(6). doi:

Acknowledgements

The authors would like to thank the LPC Caen for the loan of FASTER acquisition module and Dr. Elisa Grimoin for the help with the two-photon imaging system. CNRS, CEA, Université de Caen-Normandie, the French Ministère de l'Enseignement Supérieur et de la Recherche, the Conseil Régional-Normandie and the European Union-Fonds Européen de Développement Régional (FEDER), the Fédération pour la Recherche sur le Cerveau par l'opération Rotary "Espoir en tête » (FRC), ANR-11-LABEX-0018-01 ; ANR-10-EQPX1401. MSS, NRS, KAV, OT and NF were supported by Cancer Research UK (grant number C5255/A15935). Grant support was also received from the Medical Research Council (MC_PC_12004) (KAV, OT, NF), the Engineering and Physical Sciences Research Council (EPSRC)

Oxford Centre for Drug Delivery Devices (EP/L024012/1) (KAV), the CRUK Oxford Centre (OT) and the CRUK/EPSRC Cancer Imaging Centre Oxford (C5255/A16466) (KAV).

Conflict of interest:

The authors declare no conflict of interest.